COBEM 2021 26th International Congress of Mechanical Engineering
ABCM Associação Brasileira de Engenharia e Ciências Mecânicas
November 22-26, 2021, Virtual Congress, Brazil

COB-2021-1217
HYDRODYNAMIC SIMULATION OF WECS (WAVE ENERGY CONVERTERS) FOR USE ON THE BRAZILIAN COAST.

MENDONÇA, Maria Fernanda Bezerra de.
PEIXOTO, José Ângelo da Costa.
Federal Institute of Education, Science and Technology of Pernambuco, Av. Prof. Luís Freire, 500 - Cidade Universitária, Recife - PE.
mfbm@discente.ifpe.edu.br
angelocostta@recife.edu.br

Silva, Anderson Torres de Lima; Santos, Lídia Letícia Salvino dos; Oliveira, Dayanne David Soares de; Silva, Héber Claudius Nunes; Ochoa, Alvaro Antonio Villa; Menezes, Frederico Duarte.
Federal Institute of Education, Science and Technology of Pernambuco, Av. Prof. Luís Freire, 500 - Cidade Universitária, Recife - PE.
Atls@discente.ifpe.edu.br
llss3@discente.ifpe.edu.br
ddso@discente.ifpe.edu.br
hebernunes@recife.ifpe.edu.br
ochoaalvaro@recife.ifpe.edu.br
fredericomenezes@recife.ifpe.edu.br

Abstract.: *WECs (Wave Energy Converters) are devices that convert wave energy into electrical energy. The demand for new sources of energy has been growing, such as devices are alternatives to minimize the emission of CO2 and a renewable source of energy, favoring the reduction of the use of sources such as coal and oil. Small WECs (<1kW) are a way of circumventing problems related to the high cost for implementing offshore technologies, being able to absorb energy in coasts with a slight wave regime, making it ideal for the Brazilian coast (20 kW/m on average). Therefore, the study's objective was to develop a low-power WEC for application on the Brazilian coast. After creating the float model via CAD (Computer-Aided Design), CAE (Computer-Aided Engineering) numerical simulation takes place, using Ansys Aqwa for a hydrodynamic simulation and Mechanical for the structural part. To extract data from the prototype to evaluate its performance, a hydrodynamic simulation of the geometry and two analyzes, using finite elements (FEA), of the rotor model. Data from the Pernambuco coast were used as boundary conditions. Finally, the feasibility of applying the float on the coast of Pernambuco was evaluated.*

Keywords: *Wave energy, wave energy converters, Hydrodynamic Simulation, FEA simulation, Renewable energies.*

1. INTRODUCTION

With a forecast increase in electricity consumption demand of 28% globally by 2040, developing countries will be responsible for this energy pressure (Doyle and Aggidis, 2019). WECs (Wave Energy Converters) are devices capable of transforming the energy contained in waves into electrical power. As a clean and renewable energy source, such devices can be an option to overcome the problems of a society looking for new ways to extract energy sustainably. According to the study by Espíndola and Araújo (2017), on the 8,000 km of the Brazilian coast, it is possible to generate 89.97 GW in one year, with an average wave power of 20kW/m, which shows that the resource can be successfully exploited.

Despite the wave energy dependence of wind characteristics, it is a very predictable source. It is possible to predict the characteristics of waves that reach the coast days in advance (André, 2010). However, the adversity of wave energy is seasonality, as a characteristic of renewable sources is their intermittence. Another challenge is the high cost of implementing offshore devices. Thus, a way to overcome the challenges of these technologies is to invest in small WECs (<1kW), capable of generating energy even on coasts with a slight wave regime. Thus, to analyze the feasibility of applying small WECs on the Brazilian coast, the present work used CAD (Computer-aided design) and CAE (Computer-aided engineering) tools to see how the devices behave. The CAD tool is part of creating a prototype geometry that will be tested using the Ansys Aqwa and Mechanical tools used in the hydrodynamic and structural simulations, respectively.

2. CLASSIFICATION OF WECS.

For Uihlein and Magagna (2016) there are several ways to extract energy from the oceans, one of which is wave energy. However, it is still in its initial phase, with more prominence in the research area, still requiring further study on the commercial possibilities of the devices. In this bias, the greatest demand for the source came in the 70s, considering that the 1973 oil crisis induced a major change in the renewable energy scenario and increased interest in large-scale energy production from waves (Falcão, 2009). Also, energy from waves will become popular due to rising fuel costs and fluctuating energy prices, which makes the resource promising given its stable nature (Vinning and Muetze, 2009).

Thus, WECs can be classified according to the depth of the water where they are located and according to their operating principle. For the first criterion, the devices can be of the onshore type, located on the coast, nearshore, close to the coast, and Offshore, which are devices far from the coast. As for the second criterion, we can list the WECs between devices of the CAO (Water Oscillating Column) type, floating bodies, divided between progressives and absorbing points, and Overtopping. When we classify devices according to their proximity to the coast, we consider the depth of the water, as in deeper water, the converters can reach higher powers.

Thus, from onshore WECs, some benefits are obtained, such as not needing submerged cables to conduct electricity, easier installation and maintenance of equipment, and easier access to equipment, not requiring vessels (Dantas, 2015). However, they do not enjoy wave regimes with great energy potential. The type of WEC that stands out most in this class are the oscillating water columns, which are partially submerged structures, hollow inside, arranged on the coast so that the wave meets the inner wall of its design, pressurizing the air, causing let it go through a turbine. From the movement of this turbine, energy will be generated. Nearshore WECs are located in water depths of 10 to 25 m. According to (Cruz and Sarmento, 2004), these devices can be found in structures such as breakwaters, and CAO-type devices also belong to this class.

Offshore devices are found in deeper waters and can capture more wave power. However, the challenges for this class are the big problem since it requires a higher cost for its implementation. In addition, floating body type devices are generally situated in deeper water. Another group belonging to this classification is the overtopping type devices. Overtopping devices are reservoirs filled with seawater through a type of concentrator that raises the height of waves (Garcia Rosa, 2008). The type of apparatus developed in this article belongs to this category, being equipped with a ramp and a rotor in its central part. Below, some onshore technology devices are exemplified.

2.1. Wave Dragon Device

The Wave Dragon is a wave energy converter that works on the overtopping principle. Two reflector arms are used to direct waves arriving at the ramp, filling a reservoir located above sea level. Energy is produced when water passes through low-fall turbines on its way back to the sea (Ekilsson, 2015). The Wave Dragon can reach, in full scale, a nominal power of 7 MW, in a range of 4 and 11 MW, according to the average wave climate of the Atlantic (36 to 40 kW/m) (Cruz E Sarmento, 2004b).

2.2. Archimedes swing device (AWS)

Developed by AWS Ocean Energy Ltd, have its first experimental test occurred in 2004, in Portugal. The AWS is a device that falls into the class of point absorption type floating bodies. It consists of two cylinders (float and stator) filled with pressurized air. The float that is free to move vertically and the bottom, the stator, anchored in the sea. When the wave valley passes over it, water pressure causes air to expand inside the prototype, pushing the float upwards. When the wave peak passes through the device, the pressure causes the float to descend (Gieske, 2007). This movement is enough for the WEC to generate energy with a power of 5 MW.

2.3. Pelamis device

Authored by the company Ocean Power technology, the first test of the device was made in New Jersey and the device had a power of 40kW. The OPT Power Buoy is a floating point absorber device formed by a float and a spar. Due to the movement of the wave, the float moves and through the mechanical actuator the movement is conducted to an electrical generator. The OPT Power Bouy is also equipped with an energy storage system consisting of state-of-the-art batteries (Edwards and Mekhiche , 2014).

Furthermore, several works highlight the importance of testing WEC prototypes, such as in the studies by Bergillos (2019) and Rosa-santos *et al.* (2019) that show the importance of computer simulation in the construction of wave energy converter device designs. Bosma and Lewis et al (2015) combine computer simulation with the ability to obtain important data about the prototypes to implement them at sea.

In one study, Seibt *et al.* (2017) show the similarity between the computational modeling of a full-scale submerged horizontal plate-type wave energy converter and its laboratory-scale model. Through the method Volume of fluid (VOF)

and finite volumes, a considerable similarity was obtained between the models, considering that the highest percentage of difference shown was the average of 2% between the efficiencies of both models.

3. METHODOLOGY.

To similar the WEC, CAD, and CAE tools were used. First, the WEC geometry is created in the SolidWorks CAD software.

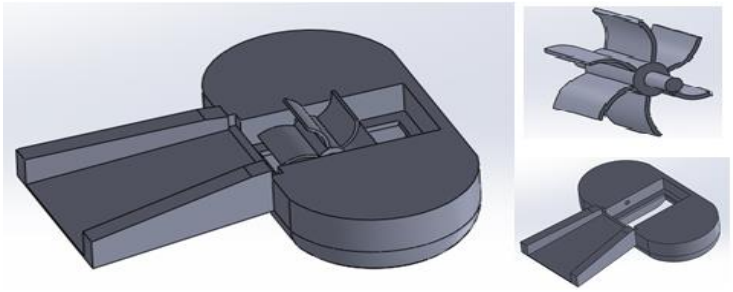

Figure 1. WEC 1.

Figure 1 shows the geometry of the prototype. In its structure, it is possible to see a ramp that serves to raise the waves and direct them to the inside of the same, where the rotor is. From the moment the water passes through the rotor, the rotational movement takes place, which generates mechanical energy to generate electrical power. The rotor structure is designed so that it generates energy through rotation as the wave passes through it. It is located in the innermost part of the WEC, where there is an opening through which the water flows and returns to the sea. For the prototype to float, its underside is inspired by maritime structures such as boats and ships.

3.1. Numerical Simulation

Numerical simulation of geometry takes place using the Ansys Aqwa and Ansys Mechanical tool. Initially, modifications are made within the cad tool of the simulation software; they consist of transforming the geometry into a shell and delimiting a waterline, defined by the XY plane, which will create a division in the structure defining the immersed and submerged part of the same. Then, the mass point data are entered, and the computational mesh is generated. Geometry mass point data is taken from Solidworks. The mesh generated in this work, was made in ANSYS Meshing and had a tolerance of 0.2 and the maximum element size of 0.05 mm, generating 8221 nodes

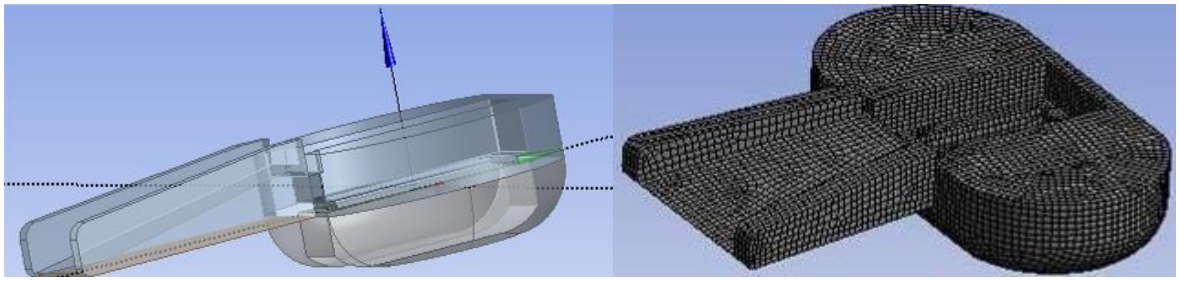

Figure 2. Structure division and computational mesh.

In the simulation setup configuration, the defined boundary conditions were the wave intervals, from -180º to 180º, which resulted in 9 directions. The number of 20 wave frequencies to be used in the analysis was also defined at this stage. These data concern the hydrodynamic diffraction part of the simulation; they will be used in the hydrodynamic response, the study of displacement, pressure, and movement data, among other results obtained in the previous phase. The sea area used in the software was 5x5 m, with a water density of 1025 kg/m3, depth of 20 m, and gravitational acceleration of 9.80665 m/s2. In addition, a five m/s wind load and an irregular Pierson-Moskowitz wave spectrum were added. The spectrum defines a relationship between the distribution of wind and energy given by Eq. (1). An average period of 12 seconds and a wave height of 0.2 m were added to use this spectrum. Below you can see the equation, where S is the spectral coordinate of the frequency, Tz is the average period, and Hs is the significant wave height.

$$s(\omega) = \frac{1}{2} * \frac{Hs}{4\pi Tz^4} * \left(\frac{2\pi}{\omega}\right)^5 * e^{\left(\frac{-1}{\pi Tz^4} * \frac{2\pi}{\omega}\right)^4} \quad (1)$$

All wave data used were based on data analysis of the Pernambuco coast. Extracted from the average of the values in a wave over 7 days, with values measured four times a day.

After the complete hydrodynamic simulation of the prototype, the numerical simulation of the rotor took place. The rotor is a structure that rotates around its axis to generate mechanical energy that will soon be converted into electrical energy. The modal and structural analysis that occurred are made via finite elements (FEA). Initially, it was unnecessary to make any changes to the geometry, so the simulation was directed to setup.

3.2. Structural analysis

The rotor structure receives efforts during the entire prototype operation. For this reason, under boundary conditions, a force of 839 N was added across all blades. This value was based on the average of the force present in a wave over 7 days. Two brackets fixed at the ends of the frame were also added to represent the most critical loading situation on the rotor. For this study, a mesh of 26,058 nodes and 13,927 elements was generated.

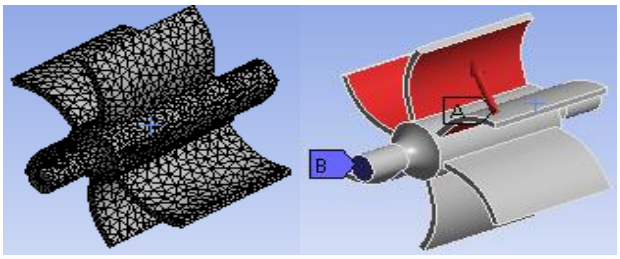

Figure 8. Computational mesh, strength, and fixed support on the structure.

3.3. Modal Analysis

After a coupling was made to the structural analysis, the modal analysis of the rotor structure can be started. In this type of simulation, it is possible to print the natural frequencies of the design and its vibration modes. Due to the coupling, the mesh used was the same one generated previously in the structural analysis. However, for its boundary conditions, only the structure fixations were used.

For the study, four different materials were used: SAE 1020 steel, 290 GPa carbon fiber, E-glass, and 1060 aluminum alloy. For each material, six natural frequencies were printed and with them their vibration modes. This part of the study evaluated the best material for the rotor structure about its vibrations.

4. RESULTS

The first result obtained is pressure and movement. In this study, it was possible to see the values obtained in the analyzes performed in Ansys Aqwa. It shows the pressure to which the structure is exposed for different amplitudes at the chosen wave frequency. To visualize these data, three-wave amplitudes were determined, being the incident direction of 90º, which directly goes against the front part of the structure and the chosen frequency of 0.50863 Hz.

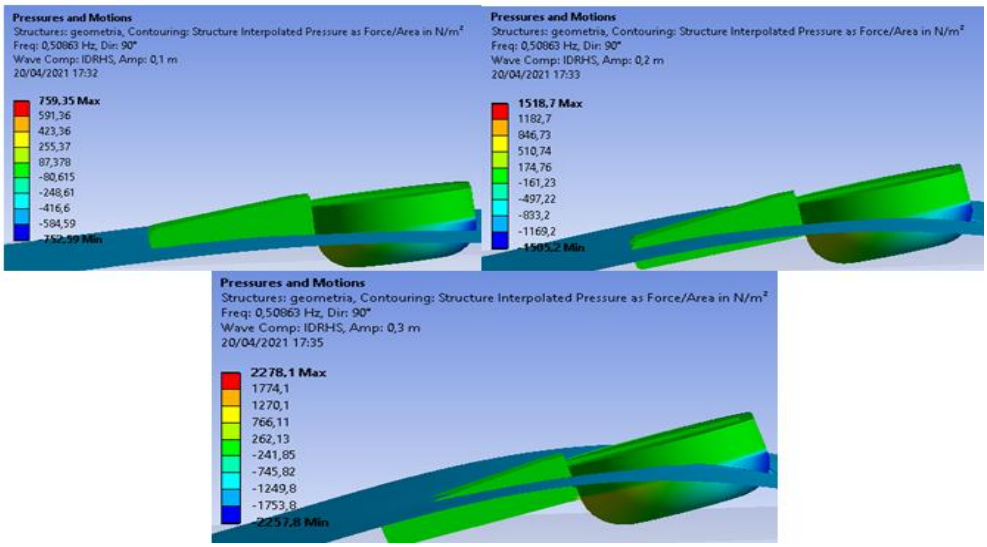

Figure 10. Pressures according to amplitude.

As in the images, the pressure, given in N/m^2, remains between the mean values in most of the structure, reaching the minimum value in the posterior part and the highest values in the region below the ramp.

Table 1. Pressures according to amplitudes.

Amplitude (m)	**Maximum (N/m^2)**	**Minimum (N/m^2)**
0,1	759,35	-752,59
0,2	1518,7	-1505,2
0,3	2278,1	-2257,8

Another result obtained was the structure's air gap. It provides the vertical distance between the points on the design and the sea line. This result used the same wave direction as the previous study and a single amplitude of 0.2 m; however, three frequencies were used: 0.01592 Hz, 0.38545 Hz, and 0.50863 Hz.

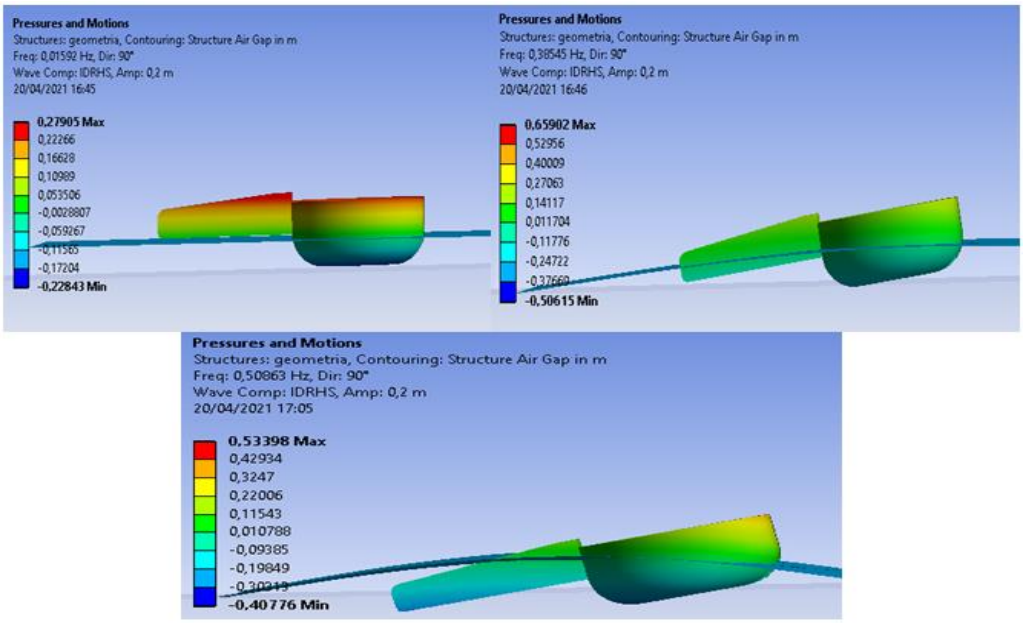

Figure 11. Structure air gap.

From the hydrodynamic diffraction stage, displacement, acceleration, and velocity results over time were also obtained. These studies were done using the 300-second simulation time, the previously defined Pierson-Moskowitz irregular wave, and a 5 m/s wind.

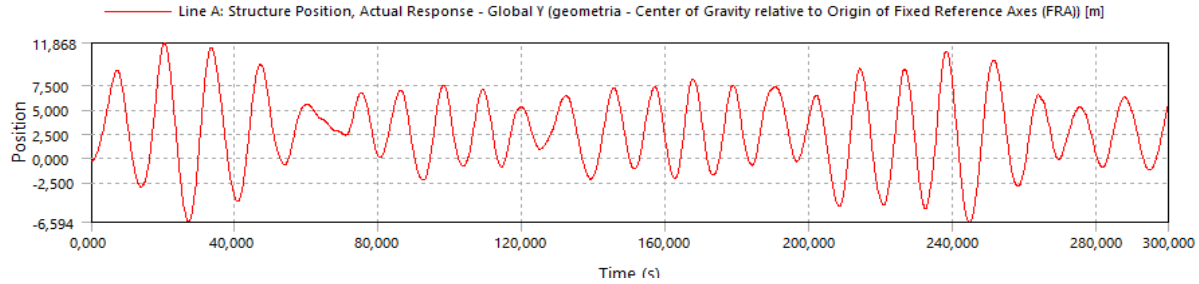

Figure 12. Displacement of structure as a function of time.

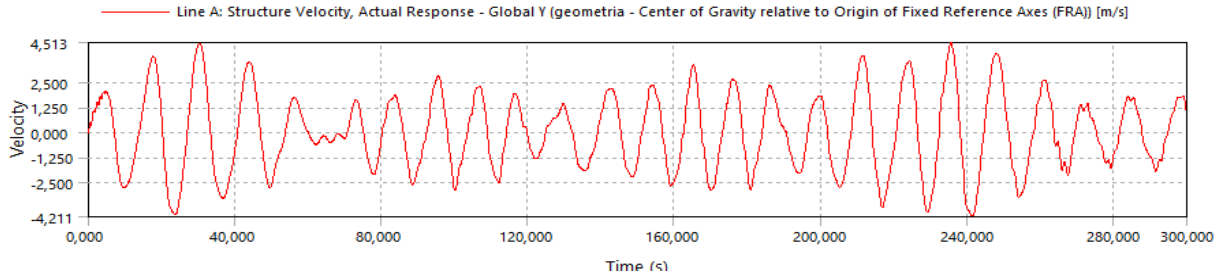

Figure 13.Variation of structure velocity over time.

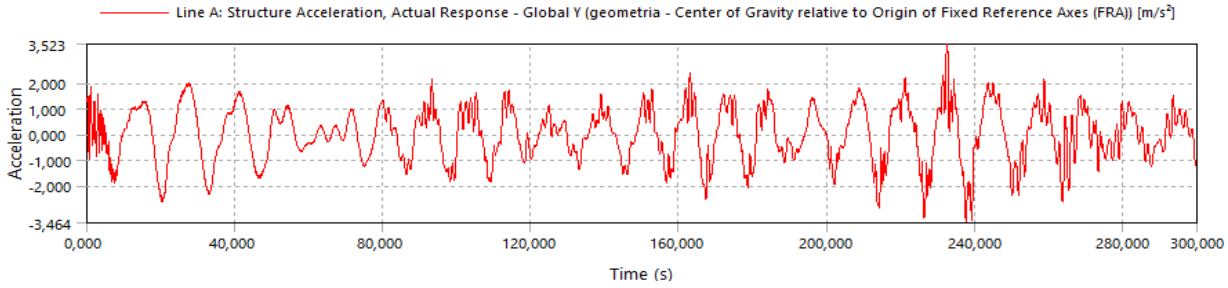

Figure 14. Acceleration variation over time.

In Figure 12, it is possible to see that the displacement of the structure oscillates as the waves pass through it, reaching a maximum point of 11.868 m. It is resulting in a final velocity of 0.99214 m/s and an acceleration of -1.03968 m/s2. To measure the vertical oscillation of the structure, the result of oscillation on the z-axis is used, highlighted in Figure 15. The smallest values refer to the instant when the system passes through the wave valley, and the largest to the moment it crosses the crest. Thus, the vertical displacement variation was between 0.8 m and -0.343 m, presenting a more significant oscillation in the first 10 seconds.

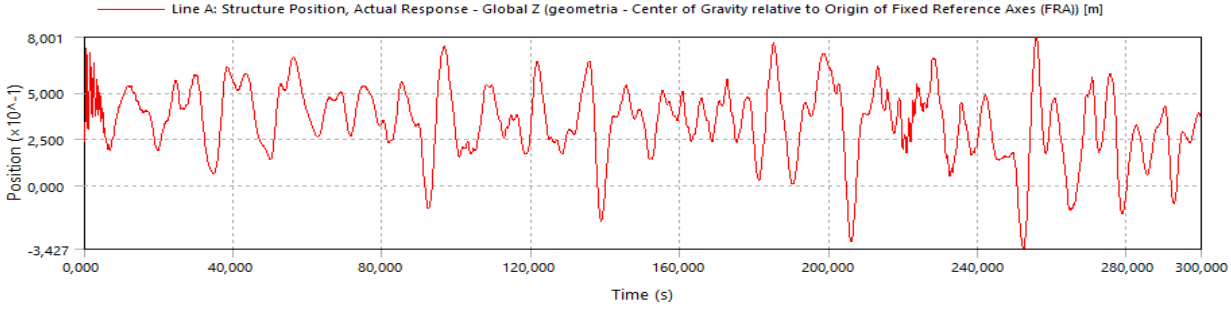

Figure 15. Vertical displacement as a function of time.

As for the structural simulations, the four materials had few differences in stress and strain values. The images below show the results in the following order: Steel SAE 1020, Carbon fiber 290 Gpa, E-glass, and aluminum 1060.

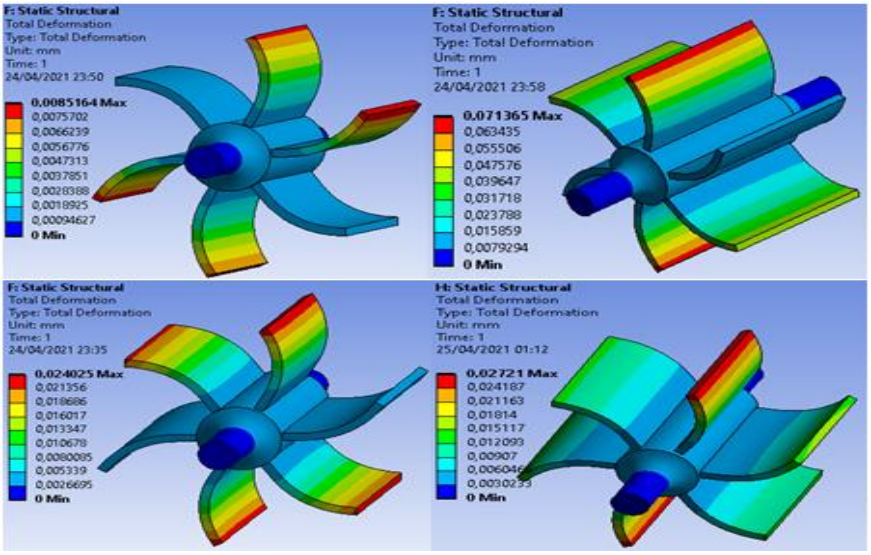

Figure 14. Deformation in the structure.

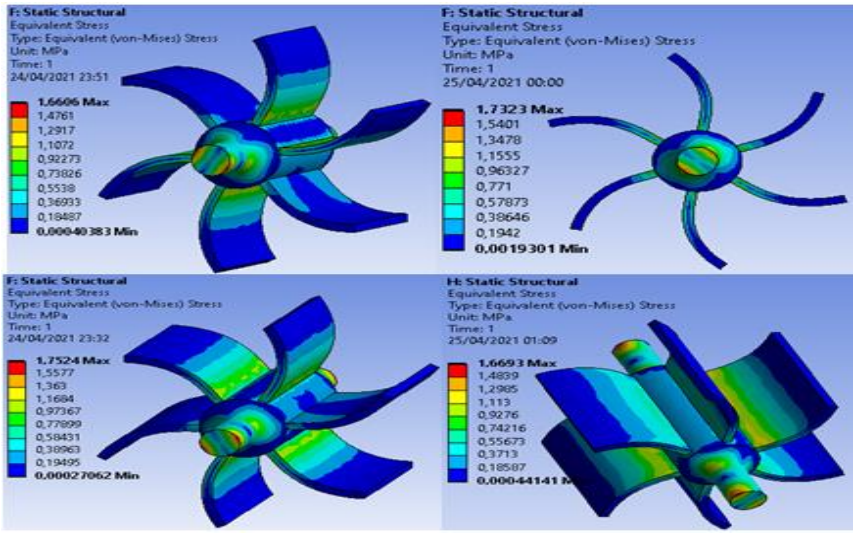

Figure 15. tension in the structure.

Table 2. Deformation and stress values.

Material	Deformation (mm)	Tension (MPa)	safety coefficient
SAE 1020 steel	0,024025	1,6606	3
Carbon fiber 290	0,071365	1,7323	2,5
E-glass	0,024025	1,7524	2,5
1060 Aluminum	0,02721	1,6693	3,5

The deformation points in the structure present maximum results in the blades in both simulations, and the stress results, as it is a free region to move, give smaller values in the blades and more significant in areas where the structure is fixed. As the loading for each material was the same, the stresses had similar results.

As for the modal analysis, the vibrate modes and the six natural frequencies (Hz) can be seen in the images below.

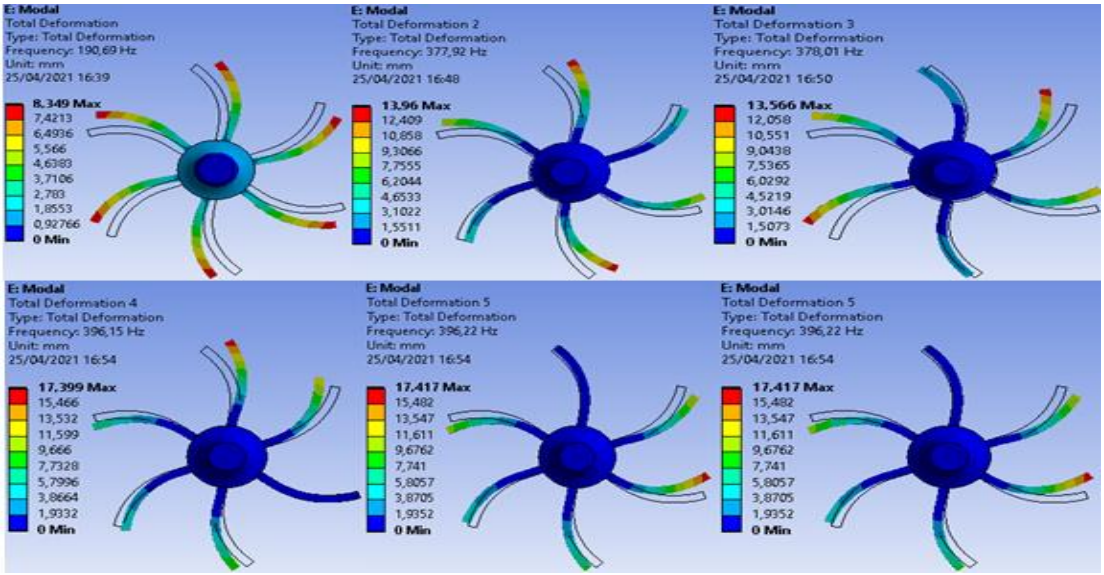

Figure 16. Natural Frequencies and Vibration Modes of Structural Steel.

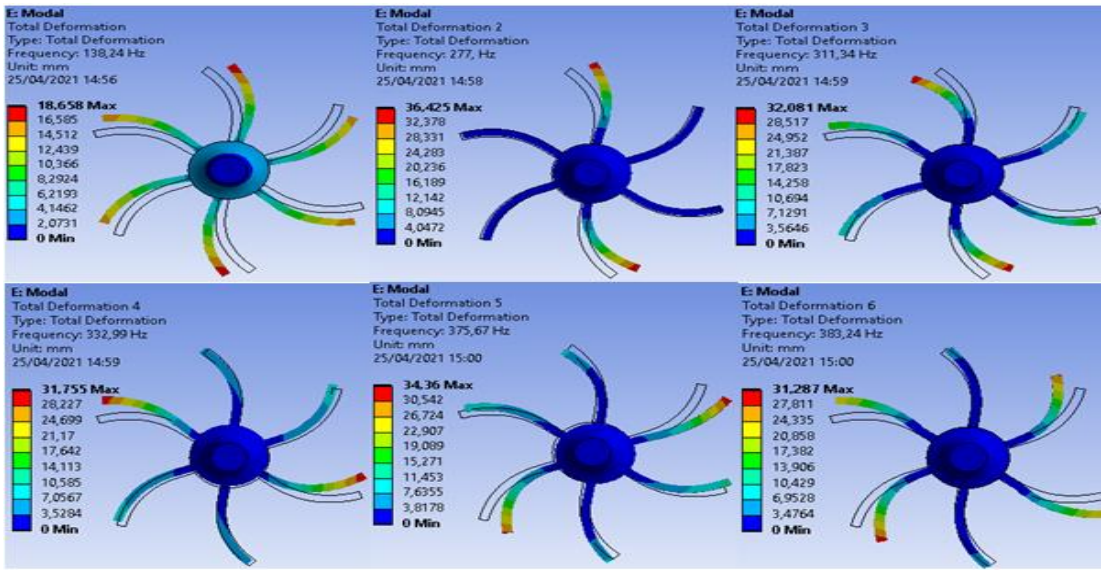

.

Figure 15. Natural frequencies and vibration modes of carbon fiber.

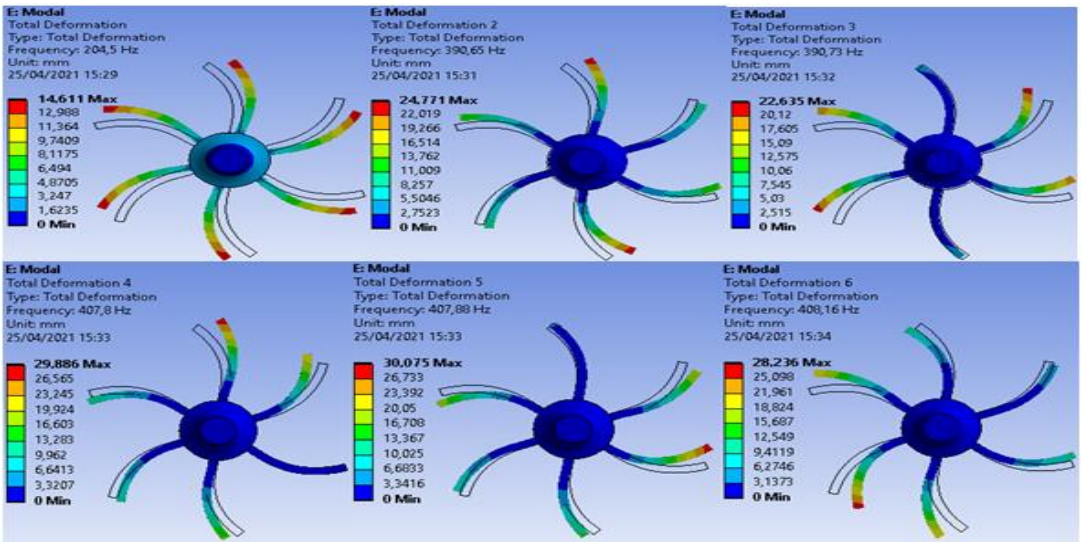

Figure 17. Natural frequencies and modes of vibrating fiberglass

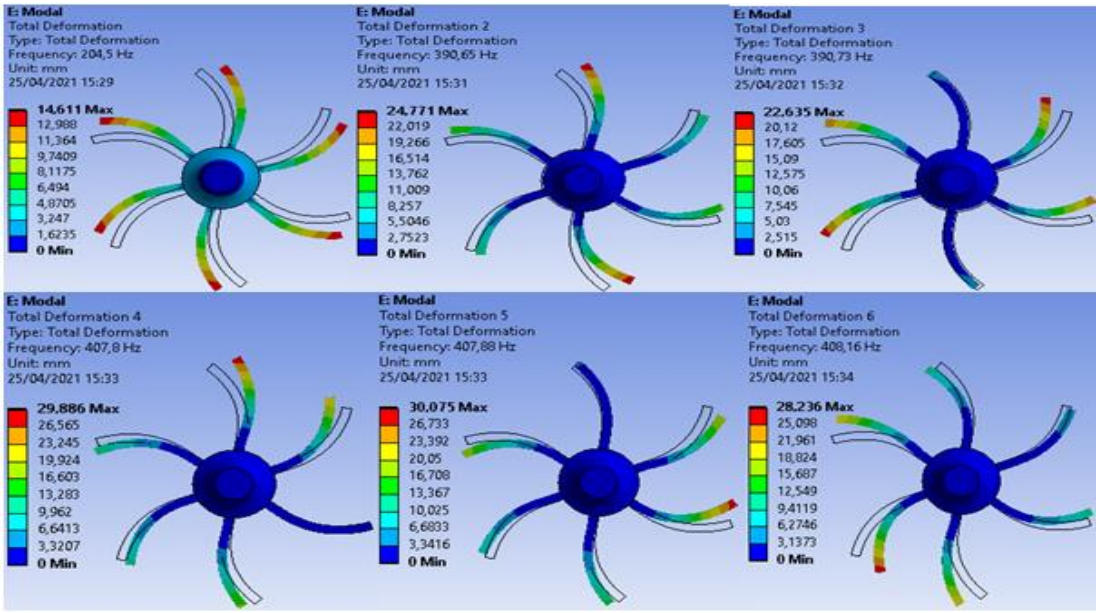

Figure 18. Natural frequencies and vibration modes of aluminum.

The four materials were also compared according to other criteria. Table 3 shows the evaluation criteria and the respective values for each material:

Table 3. Specific mass, cost per kg, yield limit and modulus of elasticity of materials.

Material	Mass (g/cm^3)	cost (R$)	flow limit (MPa)	Elasticity limit (GPa)
SAE 1020 steel	7,81	2,17	210	200
290 carbon fiber	1,8	275,15	960	290
E-glass	2,55	41,90	2400	73
1060 Aluminum	2,7	3,70	90	69

In terms of strength, all materials showed satisfactory results. However, structural steel has a higher value than others, which is a negative criterion for it. As for prices, carbon fiber and glass fiber presented very high values, not economically viable for small-scale production, despite their high mechanical strength. Thus, based on the previous results and the factors mentioned above, the material chosen for the rotor is aluminum. It stands out for being more economically viable and lighter. It is also a material with easy access and handling, which makes it ideal for the project.

5. FINAL CONSIDERATIONS

From the simulations, it was possible to evaluate the displacements, velocity, and acceleration in the structure when exposed to environmental loads used as boundary conditions. According to the vertical oscillations, it is possible to see that the design did not sink during the 300 seconds of the simulation; however, a study on the anchoring for the structure can be done in further research due to the displacement suffered by it. Likewise, a coupling between Aqwa and Mechanical results can be done later to get more results about the structure.

As following challenges, experimental tests and studies on structural loads of the complete geometry may occur to analyze the structural effect of the pressures suffered in the prototype, its energy values, and possible optimization. In the modal results, the steel showed a deformation at each frequency a little lower; this is due to the specific weight of the material being higher than the others. Frequency is directly related to the number of revolutions per minute. Thus, the four materials reached a very high-frequency range, being susceptible to a more detailed future analysis regarding the rotor rotations.

6. ACKNOWLEDGEMENT

The authors (Ochoa, A.A.V) thank the IFPE for its support for research project. The seventh author thanks the CNPq for the scholarship of Productivity nº 309154/2019-7.

7. REFERENCES

ANDRÉ, R. A. A. Modelação de um sistema de conversão de energia das ondas. 2010. 132 f. Dissertação de mestrado(Mestrado Integrado em Engenharia Mecânica) – Universidade do Porto, Porto, 2010.

BERGILLOS, R. et al. Wave energy converter configuration in dual wave farms. Ocean Engineering, v. 178, p. 204–214, 2019.

BOSMA, B.; LEWIS, T.; BREKKEN, T.; VON JOUANNE, A. Wave Tank Testing and Model Validation of an Autonomous Wave Energy Converter. *Energies* 2015. Available in: https://doi.org/10.3390/en8088857.

CRUZ, J. M.; SARMENTO, A. J. 2004. Energia das ondas: introdução aos aspectos tecnológicos, económicos e ambientais. Portugal: Instituto do Ambiente Alfragide.

DANTAS, C.E.B. Estudo dos conversores de energia ondomotriz em energia elétrica. Universidade de Brasília. Brasília, 2015.

DOYLE, S.; AGGIDIS, G. A. ,2019. Development of multi-oscillating water columns as wave energy converters. **Renewable and Sustainable Energy Reviews**, v. 107, p. 75– 86.

EDWARDS, K.; MEKHICHE, M. Ocean power technologies powerbuoy®: system-level design, development and validation methodology. Seattle, 2014.

ESKILSSON, C. & PALM, J.; KOFOED, J.P.; FRIIS-MADSEN, E. CFD study of the overtopping discharge of the Wave Dragon wave energy converter. Renewable Energies Offshore. p. 287-294, 2015.

ESPINDOLA, RL: ARAÚJO, A.M., Wave energy resource of Brazil: An analysis from 35 years of ERA-Interim reanalysis data. PLoS ONE 12 (8): e0183501,2017.

FALCÃO, A. F. de O. "Wave energy utilization: A review of the technologies". Elsevier: Renewable and Sustainable, v. 14, p. 899-918, 2009.

GARCIA-ROSA P. B.; LIZARRALDE F.; CUNHA, J. P. V. S., 2008. **Controle de velocidade de uma turbina para um sistema de conversão de energia das ondas**. Rio de Janeiro, Brasil.

GIESKE, P. Model Predictive Control of a Wave Energy Converter: Archimedes Wave Swing. MS thesis, Delft University of Technology, Delft, The Netherlands. 2007.

ROSA-SANTOS, P. et al, 2019.The CECO wave energy converter: Recent developments, **Renewable Energy**, v. 139, p. 368–384.

ROSA-SANTOS, P. et al, The CECO wave energy converter: Recent developments, Renewable Energy, v. 139, p. 368–384,2019.

SEIBT, F.M.; COUTO, E.C.; DOS SANTOS, E.D.; ISOLDI, L.A.; ROCHA, L.A.O. Modelagem computacional do conversor de energia das ondas tipo placa horizontal submersa em escala real e análise de similaridade com modelo em escala de laboratório**. Revista Brasileira de Energias Renováveis**, v.6, n.3, p. 397-418, 2017.

UIHLEIN, A.; MAGAGNA, D. Wave and tidal current energy – A review of the current state of research beyond technology. **Renewable and Sustainable Energy Reviews**, v. 58, p. 1070-1081, 2016.

VINING, J.G.; MUETZE, A. Economic factors and incentives for ocean wave energy conversion. IEEE Transactions on Industry Applications, v. 45, n. 2, p. 547-554, 2009.

8. RESPONSIBILITY NOTICE

The authors Maria Fernanda Bezerra De Mendonça, José Ângelo Da Costa Peixoto, Anderson Torres De Lima Silva, Lídia Letícia Salvino Dos Santos, Dayanne David Soares De Oliveira, Héber Claudius Nunes Silva, Alvaro Antonio Ochoa Villa, Frederico Duarte Menezes are solely responsible for the printed material included in this article.